Evaluation of Ground Systems Performance on Rail Potential and Stray Current in Tehran Railway System

Ebrahim Zare Juybari[1]* and Ahmad Gholami[2]

Abstract— **DC Stray currents represent serious problems for any electrified railway system. This paper describes a complete simulation model for evaluating rail potential and stray current for the Tehran multi-train DC railway system based on different earthing systems. In the present paper, a complete analysis of the results is presented. The simulation results clearly indicate that earthing system arrangements and other parameters influence stray currents and rail potential. The simulation results show the performance of three ground system types: grounded, ungrounded, and diode-grounded systems on rail potential and stray current.**

Index Terms— DC Railway System, Multi-Train Simulation, Rail Potential, Stray Current, Monte Carlo Simulation

I. Introduction

Most railways systems use the running rails as the return conductor for traction current to reduce the wiring cost. The disadvantages of such an arrangement are those of rail potential and stray current problems [1, 2]:

- Rail potential may rise or fall above a certain threshold and can be hazardous in the forms of touch or step voltages. Rail potential should not exceed the critical value of correlative standards to avoid endangering the person's safety.
- Stray currents can dramatically create or accelerate the electrochemical corrosion of underground metallic utility pipes, power and telephone cables and the earthing grids laid in the vicinity of the DC railway system.

Therefore, controlling rail potential and stray current is important in all DC railway system designs. Rail potential and stray current are influenced by factors such as the conductance per unit length between running rails and earth, rail resistance, distance between traction substations, line voltage, weather, position and loads condition. Among them, the earthing strategies profoundly influence both rail potential and stray current [3, 4].

The present paper deals with modeling and simulation of a multi-train DC railway system to determine rail potential and stray current values in different structures (earthing strategies) for different conditions of the Tehran metro system. The metro is used with a direct current power supply for short distances in urban transportation. An alternating current power supply is suitable for distances of more than 30 km between two stations, and for distances over 200 km, magnetic levitation trains are used [5, 6]. Stray currents that crawl through rails into the earth can flow through building foundations, pipes, and other underground metallic installations with less resistivity concerning the soil to reach the negative terminal of the substation. The points at which current enters/leaves the metallic structure are called the cathodic/anodic regions [7- 9]. The current leaving the anodic region causes the corrosion phenomenon on the metallic structure. Various methods have already been used for stray current modeling in railway transit systems. In most of the literature and simulations, such as in [10- 12], the metro system is presented as resistive grids, and the mathematical equations are given based on the traction substation current, rail track resistance, the distance between the train and substation, the resistance between the rail and earth, and stray current. In summary, the contributions of the study are as follows:

• Analysis and comparison of different types of metro ground systems by TPS and ENS simulation;

• Presenting and comparing the effect of longitudinal resistance of running rails conductivity of rails to ground on stray current and rail potential;

The rest of the paper is organized as follows. Section 2 applied the Block diagram of train motion equations and presented mathematical and analytical relationships. Section 3 Speed and power simulations are performed for the DC metro line in Tehran. In Section 4, the simulation results obtained from the software are studied and analyzed.

II. Modeling and Simulation of DC Electrified Railway System

Simulation of the railway system is complicated for its multiple nonlinear and time-varying equalities. Because it is composed of many components, the relation between them changes in time. Anyway, the Simulation of the DC Electrified Railway System was conducted in the following three stages:

• Train performance simulation
• Electric network simulation

1- Electrical Engineering Faculty, Imam Mohammad Bagher, Technical and Vocational University, Mazandaran, Iran

2- Electrical Engineering Faculty, University of Science and Technology, Tehran, Iran
Corresponding author: ebrahim.zare.juybari@gmail.com

• Rail potential and current ground simulation

2.1 Train Performance Simulation

2.1.1 Train Motion Equation (TME)

Train motion can be best described by Lomonossoff's equation [13, 14]:

$$(M + DM)\frac{dv}{dt} = TE - (a + bv + cv^2) - Mg(\alpha - \alpha') \quad (1)$$

Where M is the mass of the train, DM is the dynamic mass of the train (typically 5%-10% of M), v is train speed, TE is tractive effort, "a,b,c" are running resistance coefficients of the train, g is gravity, α is a slope at the current position, and α' is the curvature at current position converted to equivalent slope according to the following:

$$\alpha' = \frac{\mu(L+G)}{2\times R}\times 10^6 \quad (2)$$

Where G is track gauge (m), L is axial length (m), R is the radius of curvature (m), and μ is wheel-rail adhesion coefficient. The adhesion coefficient is empirical and can be approximated by Curtius Kniffler's formula for "dry rail" conditions [13, 14].

$$\mu = 0.161 + \frac{7.5}{44 + 3.6v} \quad (3)$$

The running resistance coefficients depend on the number of axles, total train length, and train cross-section area. The tractive effort of electric locomotives depends on various factors but mainly on the weight and speed of the train. For metro operations with a high passenger density, the variation in train weight can significantly affect train performance and energy consumption. With a time-based (time of day) passenger profile for each station, the weight of trains can be altered [14, 15].

Usually, the locomotive tractive effort determines as a function of speed and line voltage. Therefore, for each time snapshot, the output mechanical power of the train (motors) is obtained by equation (4). The total input electrical power (P_{tot}) of the locomotive measured at the pantograph is calculated by equation (5). The auxiliary power, electrical losses and mechanical losses, as well as all other losses, are included in P_{tot} [14, 15, 16]:

$$P(v) = TE(v)\times v \quad (4)$$

$$P_{tot} = \frac{P(v)}{\eta_t} \quad (5)$$

$$I(v) = P_{tot}(v)/V_{dc}(v) \quad (6)$$

Where $P(v)$ the tractive power, η_t the total power efficiency; $V_{dc}(v)$ the supply voltage of the train,the train current.and $I(v)$

Train motion equations (*TME*) are then solved using the built-in integration methods equipped with the algebraic loop solver to account for train speed, position, and line voltage effects. The Block diagram of single train dynamics is shown in Fig. 1. It consists of three major modules, i.e., the Trains Performance Simulator (*TPS*), the Electric Network Simulator (*ENS*), and the Train Movement Simulator (*TMS*). The railway system's operation timetable (T-V* profile) is applied to define each train's location and speed profile along the main line for each time snapshot. In reality, the *T-V** profile corresponds to either the speed code received from the track signaling system or the speed demand set by the driver during operation. The speed control module produces the desired *TE / BE* to achieve the desired speed. The desired *TE* demand is only subject to acceleration and jerk limits [12, 14].

The actual speed and position are computed using the train motion equation (*TME*). Traction power (*TE*) or braking power (*BE*) is obtained by equation (4). If trains use an inverter propulsion system, then the efficiency characteristics are used to calculate the electric power demand. Similarly, train regeneration power output can be obtained from efficiency characteristics [12, 14].

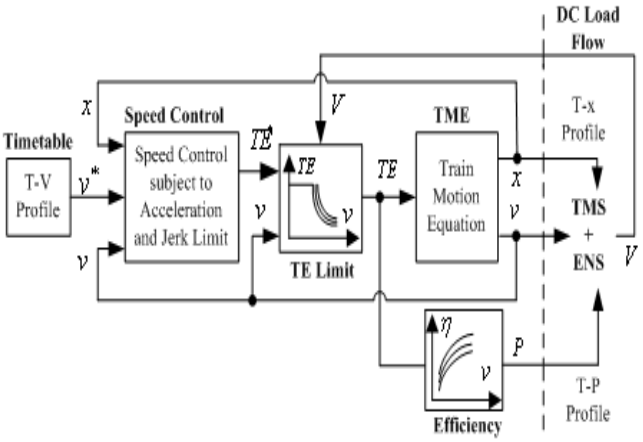

Fig. 1. Block diagram of train motion equations as related to *TPS*, *TMS*, and *ENS*

2.1.2 Monte Carlo Simulation of Operation Timetable Delays

The Monte Carlo method is a stochastic simulation technique implemented to solve a category of problems dealing with the variables of random nature [17]. Timetable delays per train are considered as the random variable in this study. Obviously, the probability that a train leaves the station with delay is much more than that it leaves at the scheduled time (T_{sch}). Therefore, triangular or normal distribution for this variable (the departure time) is a proper choice. The simulator output will include the number of trains of each line (headway), timetable delays per train, delays per trip, total and average delays and average and maximum speed. This information is available as a "per train", "per day" or summary output.

2.1.3 The AC/ DC Power Supply System Model

The power supply system is one of the most important facilities in electric railway systems. It provides the necessary energy for the operation of trains and the load at stations and depots. The Bulk Supply Substations (BSS) connect the railway power supply system to the national supply at several locations and step the high-voltage (63 kV) down to medium-voltage (20 kV). Then, it distributes a 20 kV supply to the traction supply

substation (TSS), the Station Supply Substations (SSS), and the depots. In TSS**,** 20 kV voltage is stepped down to low-voltage (592V AC) and (12 pulses) rectifiers are used to convert the AC power supply to 750 (780) V DC power source for train sets [18].

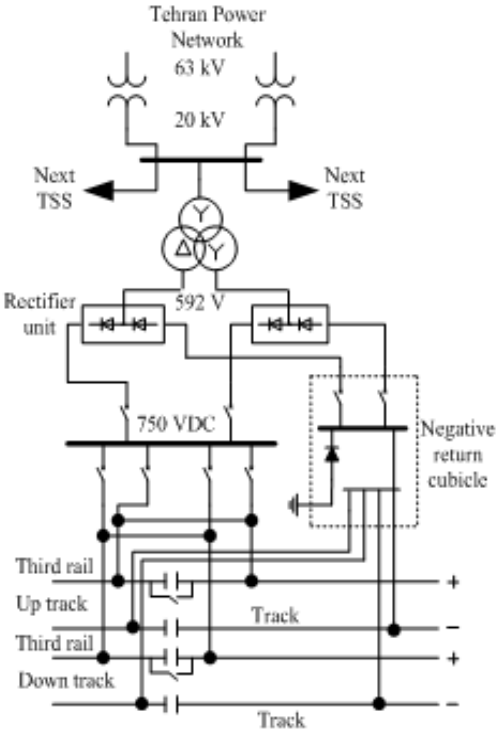

Fig. 2. Power supply system of propulsion traction for Tehran railway system

As shown in Fig. 2, the positive bus of TSS is connected to the third rail and the negative bus to the running rails. To prevent cathode corrosion phenomena due to the stray current, the negative return of DC is collected by the running rail and connected to the negative terminal of the rectifiers in TSS.
The train sets, operated along the main lines, pick up DC power from the third rail for traction motors to drive the train set.

2.1.4 Traction Motor Model

For each train set, several units of motors (DC motors or three-phase induction motors with VVVF[1] inverters) are used to provide propulsion power. An equivalent motor is used to represent several traction motors in each train. The motor has an equivalent rating (voltage, power, etc.).

2.2 Electrical Network Simulation

Having obtained the location and power consumption data for each train, the equivalent electrical network for each snapshot or specific time can be configured, as shown in Fig. 3. Each train set is treated as a load bus in the load flow analysis, and the number of train sets to be put into operation for each metro line is determined by scheduled headway. The impedance matrix of the DC network is updated according to the actual locations of all train sets. There are several methods to solve a railway traction power network. Then the voltage drop or power flow can be evaluated by electrical network simulation (ENS), which leads to the current flow into or out of the train, depending on the train's operation mode (i.e., acceleration, constant-speed, or deceleration). The current outflow from each traction substation (TSS) was also evaluated. Then, the rail potential and current ground simulation were followed by simulating each substation as a current source and each train as a current sink or a current source, depending on the train's operation mode [17, 18].

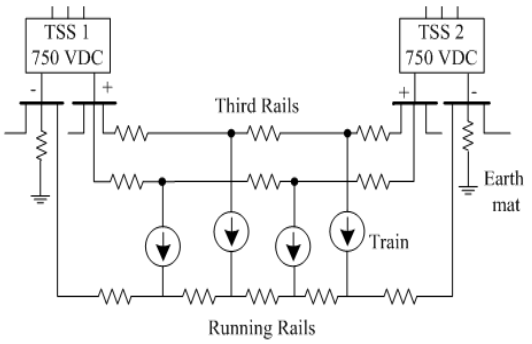

Fig. 3. Multi-train and double-tracks model of DC electrified railway at a snapshot or specific time

2.3 Rail Potential and Ground Current Simulation

The rail potential and current ground simulation were followed by simulating substations, trains, running rails, collection mats (if any), and substation grounding.

2.3.1 Running Rail Model

The rail potential and current ground equations can be obtained by a simple model based on DC transmission line equations under stationary conditions. These equations describe the system represented in Figure 4, constituted by a linear rail embedded in the soil. Where R_R is DC rail resistance per unit length $[\Omega/m]$, G is DC rail to ground conductance per unit length [*S/m*].
Rail-to-earth conductance can vary depending on the type of construction, amount of dirt on rail fasteners, temperature, ballast condition, and ambient moisture. If assumed that the rail is a cylindrical conductor with a radius $r_0 (<< d)$ embedded in the ground, then the conductance per unit length can be calculated as [19, 20]:

$$G = 2\pi/[\rho.\ln(2d/r_0)] \quad (7)$$

Where ρ is soil resistance $[\Omega.m]$, and d is rail length [*m*].

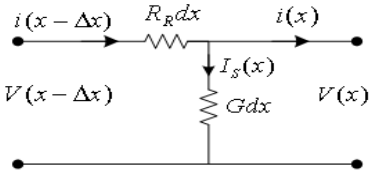

Fig. 4. DC transmission line model

2.3.2 Rail Potential and Stray Current Modeling for Multi Trains System

[1] - Variable Voltage and Variable Frequency

If rail resistance and the rail-to-earth conductance are assumed constant and homogeneous, then rail current $i_i(x)$, rail potential $v_i(x)$ and stray currentsection the inside $Is_i(x)$ $P_iP_{(i+1)}$ can be calculated as follows [4, 6]:

$$i_i(x) = c_{(2i-1)}e^{\gamma x} + c_{2i}e^{-\gamma x} \tag{8}$$

$$v_i(x) = -R_0(c_{(2i-1)}e^{\gamma x} - c_{2i}e^{-\gamma x}) \tag{9}$$

$$Is_i(x) = Gv_i(x) \tag{10}$$

$$1 \le i \le n+m$$

Where:

γ : Propagation constant (m^{-1}) = $\sqrt{GR_R}$

R_0 : Characteristic resistance of the rail conductor earth system (Ω^{-1}) = $\sqrt{R_R/G}$

$c_{(2i-1)}, c_{2i}$: Constants are decided according to specific boundary conditions (as shown in Figure 5) and using Kirchhoff's current and voltage laws.

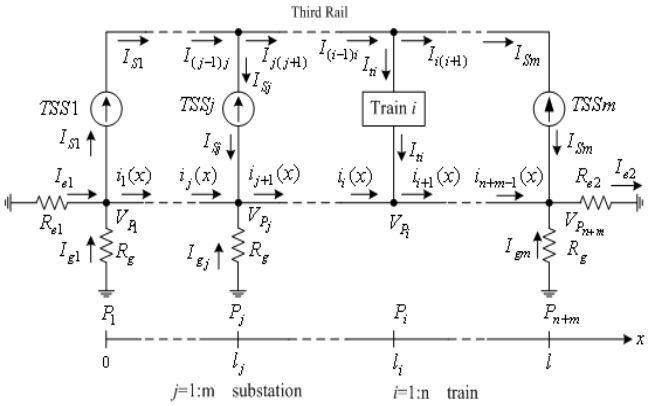

Fig. 5. Simple DC-feed multi-train rail system model at a snapshot

2.3.3 Grounding Strategies Modeling

The analytical solutions for each grounding scheme (including ungrounded, solidly grounded, and diode grounded negative return circuit) can be obtained and are useful in demonstrating the general form of rail potential and stray currents.

The analysis model of the solidly grounded traction schemes is similar to the ungrounded traction scheme, except the negative bus at each substation is directly grounded. Thus, the rail potential and stray current derivation are similar to the ungrounded traction scheme. The rail potential and stray current equations at each section are exactly the same, except for the constants (in the rail current and rail potential equations).

The analytical models of the rail potential and stray current in the diode-grounded scheme are the combined results of the ungrounded and solidly grounded schemes. The diode circuit in the diode-grounded scheme allows current to flow from the grounding mat at substations to the negative bus when a certain threshold voltage is reached. The flowchart for computations of the rail potential and stray current distribution in the diode-grounded scheme is described in reference [20, 21].

III. Tehran DC Metro Line Simulation

The performance of rail line 1 of the Tehran DC railway system is simulated to analyze rail potential and stray current. The effects of grounding strategies on rail potential and stray currents are simulated. For simplicity, we use the data from a section of line 1 (between station Q1 (Mirdamad) and station G1 (Panzdah Khordad)) for our simulation. As shown in Figure 6, this section of rail line 1 is a double-track line with a route length of 8.72km, 11 passenger stations and 5 rectifier transformer substations. The train sets, which are operated along the rail line, pick up the DC power from the third rail for their four units of 132 kW DC traction motors that drive the train set.

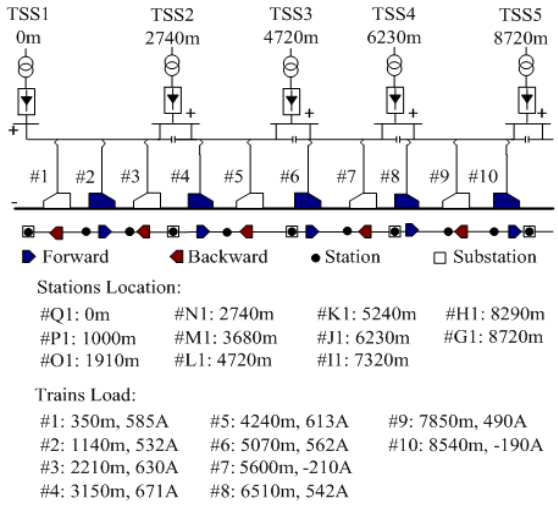

Fig. 6. The location and current consumption for the individual trains are based on an instantaneous "snapshot."

The system parameters for line 1 of the Tehran metro system are as follows: The running rail resistance is $0.035\,\Omega/km$, the rail to ground conductance is $0.02\ S/km$, and the earth resistance for the negative side of a substation grounded via the diode is $0.5\,\Omega$. The maximum slope is 5%, and the minimum radius of curvature is 250 m. The car-technical specifications are in Table I. The total run time of the train from Q1 to G1 (up-truck) is about 14 min, including 25sec of dwell time at each station. The minimum headway is designed to be 2 min [22].

TABLE I
Urban Cars-Technical Specifications of Tehran Metro Network

Number of the car per train (loco. + wagon)	7 (1+6)
Train length (m)	135
Normal static weight/ dynamic weight (tons)	341 / 363
Track gauge (m)	1.435
Front area (m2)	9.6
Number of axles	4
Starting acceleration (m/s2)	0.7
Braking deceleration (m/s2)	1.0
Max. speed (km/h)	80
Feeding voltage (Min. / Max)	750VDC (550/ 900)
Motorized car power (kW)	4*132
Auxiliary power (kW)	45

The Distance-Weight Profile for the up track under normal load is shown in Fig. 7. The Time-Speed profile for a single train in the up and down tracks (for a perfect cycle of journey) is shown

in Fig. 8, and the corresponding Time-Distance and Time-Power profiles are shown respectively in Fig. 9 and 10.

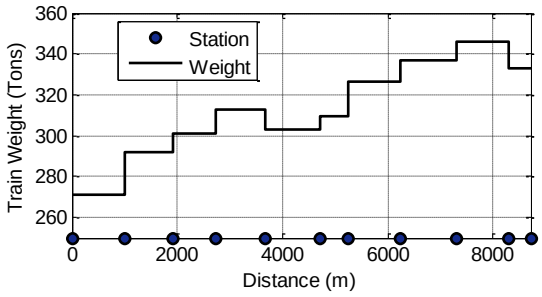

Fig. 7. Distance-Weight Profile for Up track (Normal load)

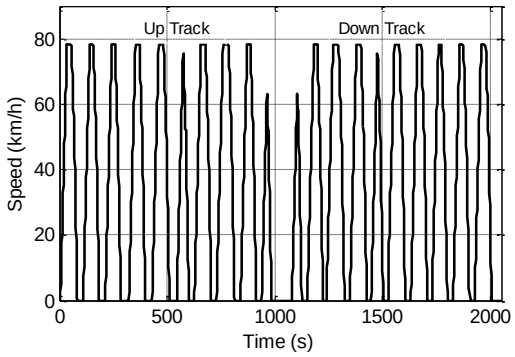

Fig. 8. Time-Speed Profile for a single train in Up and Down tracks

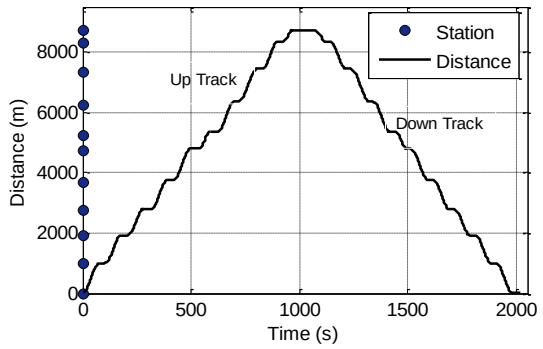

Fig. 9. Time-Distance Profile for Up and Down tracks

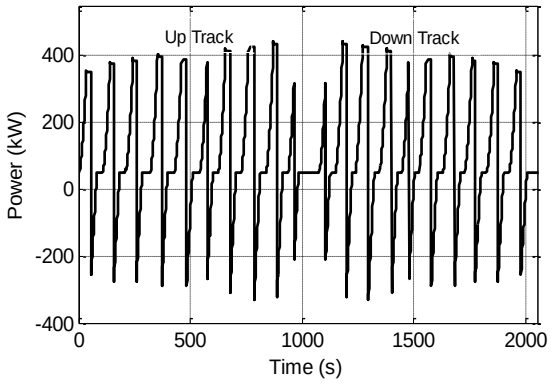

Fig. 10. Time-Power Profile for a single train in the Up and Down tracks

IV. Simulation Results and Analysis

The simulation aimed to investigate the rail potential and stray current characteristics for different earthing strategies assumed for the Line 1 of the Tehran metro system. Fig. 11, 12 and 13 depict one of the typical simulation results. This case simulated the rail potential at a typical snapshot for grounded, ungrounded, and diode-grounded systems. The locations and current consumptions for the individual trains are based on an instantaneous "snapshot" of the system (this would be determined from TPS and ENS simulation).

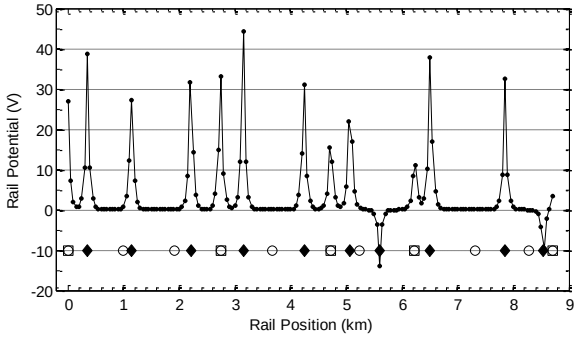

Fig. 11. Rail potential against the rail position at a typical snapshot for a grounded system

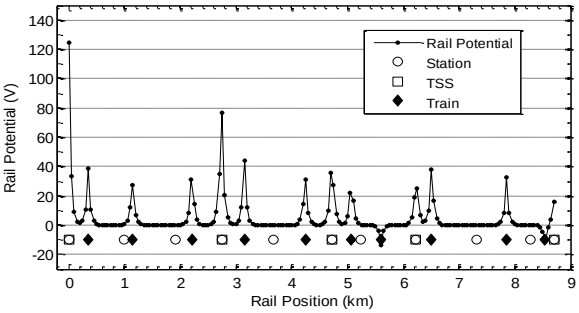

Fig. 12. Rail potential against the rail position at a typical snapshot for an ungrounded system

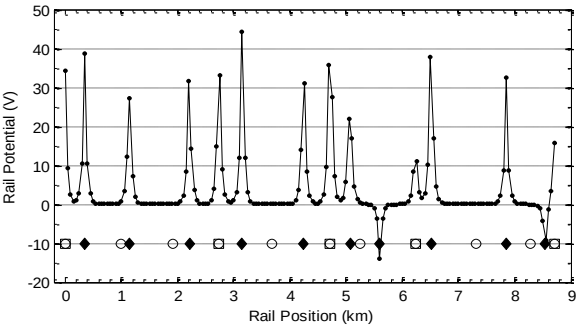

Fig. 13. Rail potential against the rail position at a typical snapshot for a diode-grounded system
(Diodes in TSS #1, 2 and 3 are turned on)

The results show that for the grounded system in some places, the rail potential increases to 45 V; for the diode-grounded system, this rail potential is up to 47 V, but for the non-grounded system in some places, the rail potential increases to 123 V.

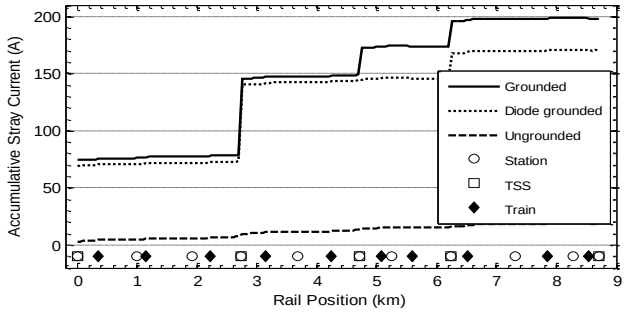

Fig. 14. Cumulative stray current against the rail position at the defined snapshot

Fig. 14 represents the accumulative stray current at a typical snapshot in grounded, diode-grounded, and ungrounded systems.

As seen in Figure 14, the accumulative stray current in solidly grounded systems is at least ten times larger than the accumulative stray current in an ungrounded system. Also, the accumulative stray current obtained in the diode-ground scheme is small compared with the result obtained in the solidly grounded scheme. Since the diode-grounded scheme represents a compromise between a solidly grounded and ungrounded traction scheme, the rail potential and stray current of the diode-grounded system are then between the other two grounding systems. The diode-grounded scheme for the DC railway system mainly depended on the number of substations having their drainage diodes turned on. According to the results of Figures 13 and 14, it can be seen that the non-grounded system, the diode-grounded system, and the grounded system have the best performance in reducing the stray current, respectively. Still, in the case of increasing the rail potential, this arrangement is quite the opposite between them.

The simulation results show that the maximum rail potentials occur in the location of trains and traction substations (TSSs). Tables II and III show that the rail potential and accumulative stray current can vary considerably with variations in assumed rail resistance, rail-to-earth leakage resistance, and substation grounding resistance (R_g).

TABLE II

Systems Grounding Versus Touch Potential and Stray Current ($R_g = 0.5\Omega$, $dx = 50m$)

Rail Data		Maximum Rail Potential (V)		Maximum Accumulative Stray Current (A)	
$R_r(\Omega/km)$	$G(S/km)$	Grounded	Ungrounded	Grounded	Ungrounded
0.035	0.04	31.4	88.2	163.6	20.0
	0.02	44.4	124.7	198.5	19.0
	0.01	62.8	176.5	235.9	18.4
0.02	0.04	23.7	66.7	159.7	19.2
	0.02	33.6	94.3	193.2	18.5
	0.01	47.6	133.9	231.0	18.1

TABLE III

Systems Grounding Versus Touch Potential and Stray Current

($R_r = 0.035\Omega/km$, $G = 0.02S/km$, $dx = 50m$)

R_g (Ω)	Maximum Rail Potential (V)		Maximum Accumulative Stray Current (A)	
	Grounded	Diode-grounded	Grounded	Diode-grounded
0.5	44.4	44.4	198.5	170.6
1.0	46.3	53.7	158.2	130.6
5.0	67.0	98.6	91.9	55.6
10.0	72.2	110.2	79.0	39.0

Generally, the most important form of stray current reduction is maintaining high rail-to-earth resistance along the lines while minimizing line resistance by cross bonding parallel track and cables and maximizing rail cross-sections.

Using running rails with larger cross-sections and higher conductivity, which have lower longitudinal resistance, reduces the maximum Rail Potential and the maximum Accumulative Stray Current.

In addition, according to equation (6), if a higher voltage (such as 1500V DC) is used in a power traction system, the current flowing in the return conductors will be smaller**.** Therefore, stray current and rail potential will be smaller.

V. Conclusion

This paper presents a computer simulation model for analyzing rail potential and stray current in a multi-train DC railway system. Based on the simulation results, the following concluding remarks have been drawn:

- Grounded system results in very high stray currents with reasonably low rail voltages.
- Ungrounded system results in very high rail potentials with low stray currents.
- Diode-grounded system results in high rail voltages and stray currents compared to an ungrounded system.
- The stray current and rail potential depend on headway, the number of trains in operation, and the length of line (distance between traction substations).
- The changes of the diode-grounded system into a partially ungrounded system can effectively reduce the stray current.
- The isolation of two cross-junction lines by disconnecting the impedance bond at the tie line or the cross-junction can also effectively reduce the total amount of stray current and the peak of rail potential.
- If higher voltages are used in the power traction system, then the stray current and rail potential will be reduced**.**

Generally, each grounding scheme provides an essential traction design for rail systems concerning rail potential and stray current. The tasks of controlling rail potential and stray

current are conflicting; therefore, a balance has to be struck between the two.

VI. References

[1] M. Niasati., A. Gholami., 'Overview of stray current control in DC railway systems', IEEE International Conference on Railway Engineering (Hong Kong), Dec. 2008.

[2] Cotton, I., and eds., 'Stray current control in DC Mass Transit Systems'. IEEE Transactions On Vehicular Technology, Vol. 54, No. 2, March 2005, pp.722 – 730.

[3] Lee, C.H., and Wang, H.M., 'Effects of grounding schemes on rail potential and stray currents in Taipei Rail Transit Systems'. IEE Proc. Electr. Power Appl., vol. 148, No 2, 2001, pp. 148-154.

[4] Ku, B.Y., Lee, C.Y., Yen, K.H., Yang, J.J., and Lin, C.F., 'Touch potential and stray current of diode grounded traction systems'. Proc. 19th Symp. Electrical Power Engineering, Taipei, Taiwan, 1998, pp. 677–681.

[5] Hao Xue., Xiaofeng Yang., Yuhao Zhou., Trillion Q. Zheng., 'Multi-interval DC Traction System Simulator for Stray Current and Rail Potential Distribution' IEEE Energy Conversion Congress and Exposition (ECCE), 2018, Portland, USA

[6] Marek Siranec., Michal Regula., Alena Otcenasova., Juraj Altus., 'Measurement and Analysis of Stray Currents' IEEE 20th International Scientific Conference on Electric Power Engineering (EPE), 2019, Czech Republic

[7] Chen Zhiguang., Zhang Xuyan., Qin Chaokui., 'Field testing and analysis of stray current interference on gas pipeline from metro maintenance base' IEEE Conference on Power, Energy, Control and Transmission Systems (ICPECTS), 2018, Chennai, India

[8] George Marulli., Ian Cook., 'Earthing and Negative Return Systems in the Melbourne DC Railway' Down to Earth Conference (DTEC), IEEE, 2018, Melbourne, Australia

[9] Guifu Du., Jun Wang., Xingxing Jiang., Dongliang Zhang., Longyue Yang., Yihua Hu., 'Evaluation of Rail Potential and Stray Current with Dynamic Traction Networks in Multitrain Subway Systems' IEEE Transaction on Transportation Electrication. 2020. Pages: 784 - 796

[10] Sheng Lin., Qi Zhou., Xiaohong., Mingjie., Amin Wang., 'Infinitesimal Method Based Calculation of Metro Stray Current in Multiple Power Supply Sections' IEEE Access. 2020, Pages: 96581 - 96591

[11] Ebrahim Zare Juybari., Reza Keypour., Mohsen Niasati., 'Voltage Distribution Indices Method to Analyze the Performance of Various Structures of Stray Current Collectors in DC Transit Lines' IET Electrical Systems in Transportation. May 2021.

[12] Sheng Lin., Yang Huangfu., Qi Zhou and Aimin Wang., 'Evaluation and Analysis Model of Stray Current in the Metro Depot' IEEE Transaction on Transportation Electrication. 2020, Pages: 1780 – 1794.

[13] M. Niasati, A. Gholami, 'Evaluation of rail potential control devices performance for control of rail potential of DC electrified railway systems', IEEE International Conference on Railway Engineering (Hong Kong), Dec. 2008.

[14] Salman Aatif, Haitao Hu, Fezan Rafiq, Zhengyou He, 'of rail potential and stray current in MVDC railway electrification system', Springer (Railway Engineering Science journal), July 2021, volume 29, pages 394–407.

[15] Ade Ogunsola, Leonardo Sandrolini, Andrea Mariscotti, 'Evaluation of Stray Current From a DC-Electrified Railway With Integrated Electric–Electromechanical Modeling and Traffic Simulation', IEEE Transactions on Industry, Nov. 2015. Volume: 51, Issue: 6, 5431 – 5441.

[16] Aydin Zaboli; Behrooz Vahidi; Sasan Yousefi; Mohammad Mahdi Hosseini-Biyouki, 'Evaluation and Control of Stray Current in DC-Electrified Railway Systems', IEEE Transactions on Vehicular Technology, Vol: 66, Issue: 2, Feb. 2017. 974 – 980.

[17] Chengtao Wang, Wei Li, Yuqiao Wang, Shaoyi Xu, Mengbao Fan, 'Stray Current Distributing Model in the Subway System: A review and outlook', International Journal of Electrochemical Science, Dec. 2017. 13(2): 1700-1727.

[18] Tzeng, Y. S., 'DC RAIL—A power system simulator for DC electrified railways. Proc. World Metro Symp., Taipei, Taiwan, 2002, pp. 332– 337.

[19] Chang, C.S., Khambadkone, A., and Xu, Z., 'Modeling and simulation of DC traction system with VSI-fed induction motor drive train using PSB/MATLAB'. IEEE PEDS 2001, Indonesia, 2001, pp. 881–885.

[20] Lee, C.H., 'Evaluation of the maximum potential rise in Taipei rail transit systems. Power Delivery, IEEE Transactions on Volume 20, Issue 2, April 2005, pp. 1379 – 1384.

[21] 'The Effects of Moisture and Ballast Contact on Electrical Isolation of Running Rail on Wood Ties and Ballasted Track'. Deleuw Cather and Company, July 1982.

[22] Yu, J.G., 'The effects of earthing strategies on rail potential and stray currents in DC transit railways'. Proc. Int. Conf. (Conf. Publ. No. 453) Developments in Mass Transit Systems, 1998, pp. 303–309.